Eur. Phys. J. B **2**, 489–494 (1998)

THE EUROPEAN PHYSICAL JOURNAL B

Buckling in a solid Langmuir monolayer: light scattering measurements and elastic model

A. Saint-Jalmes[a] and F. Gallet[b]

Laboratoire de Physique Statistique de l'École Normale Supérieure[c], 24 rue Lhomond, 75231 Paris Cedex 05, France

Received: 18 August 1997 / Revised: 9 December 1997 / Accepted: 29 January 1998

Abstract. Above a surface pressure threshold π_c, we detect a buckled state in the low temperature solid phase of a phospholipid monolayer spread at the air-formamide interface. Stable ripples are observed with a Brewster angle microscope, and light scattering provides measurements $\pi_c = 7$ mNm^{-1}, wavelength $\Lambda \approx 16$ μm and amplitude ξ of a few nm for the deformation. A model, coupling the monolayer thickness and elongation, and consistent with the monolayer texture, is also presented.

PACS. 46.30.Lx Static buckling and instability – 68.10.Et Interface elasticity, viscosity, and viscoelasticity – 68.55.-a Thin film structure and morphology

Introduction

Comparing Langmuir film behavior on different liquids gives information about their effective role on the microscopic film structure and on specific interactions between the polar heads and the subphase molecules. Amongst many liquids, formamide (CHO-NH_2, surface tension $\gamma_0 = 58.2$ mN m^{-1} at 20 °C) can be used as an alternative non-aqueous solvent to support amphiphilic monolayers [1]. The phase diagram of 1,2-distearoyl-sn-glycero-3-phophatidylcholine (DSPC) on formamide has been determined from surface isotherms, fluorescence microscopy observations and X-ray diffraction [2,3]. As on water, one observes gas, liquid, mesophases and solid phases, but not at the same relative position.

One of the differences with the phase diagram on water is that the low temperature solid phase exhibits one single structure in the full pressure range, $0 < \pi < 50$ mN m^{-1}, as can be seen by X-ray diffraction data [3]. The chains are organized on an oblique lattice and tilted towards nearest neighbors, with a tilt angle θ of about 35° measured from Bragg rod scans. The tilt remains constant over the entire pressure range, and the compression modulus ε of this rigid phase is very large ($\varepsilon = -A\partial\pi/\partial A \approx 3500$ mN m^{-1}). Notice the difference with the behavior on water, where the tilt decreases with surface pressure [4], and the compression modulus $\varepsilon = 350$ mN m^{-1} is much smaller.

Another specific feature of this solid phase spread on formamide is the spontaneous surface buckling occurring above a pressure threshold $\pi_c \approx 7$ mN m^{-1} [5]. This buckling instability was observed for the first time with a regular optical microscope: the permanent, roughly periodic, out-of-plane deformation of the surface acts as a series of alternate convergent and divergent lenses, and the layer appears as a succession of bright and dark stripes, roughly orthogonal to the compression direction [5].

We stress that, since the microscopic structure is independent of the surface pressure, the buckling instability *cannot* correspond to a structural change in the solid phase. The large compression modulus ε in this phase is believed to be a relevant parameter for the instability.

No previous report exists of such a permanent deformation on water, except for a polymerized monolayer [6] and for a monolayer made of copolymers [7].

Brewster angle microscopy

In Figure 1 we present two images obtained by Brewster Angle Microscopy (BAM) at $T = 10$ °C. They clearly show the difference between unbuckled and buckled states. In Figure 1a, $\pi \approx 0$ mN m^{-1}, and the area per molecule $A \approx 50$ A^2/mol already corresponds to the solid phase. The monolayer appears nearly uniform, except for a slight intensity modulation. We interpret this as due to domains having different tilt orientations. Taking the FFT of Figure 1a, we measured a domain size $d = 7 \pm 1$ μm, roughly constant over the sample, independent of the surface pressure, and reproducible from one sample to the other.

Figure 1b is taken right above the buckling pressure threshold $\pi_c = 7$ mN m^{-1}. As soon as π exceeds π_c, the contrast due to surface curvature rapidly increases and several stripes of typical width close to the domain size appear. They are partially oriented, perpendicular to the compression direction indicated by the arrows.

[a] e-mail: jalmes@physique.ens.fr

[b] *Present address:* LBHP- case 7056, 2 place Jussieu, 75251 Paris Cedex 05, France.

[c] URA 1306 associée au CNRS et aux Universités Paris 6 et Paris 7.

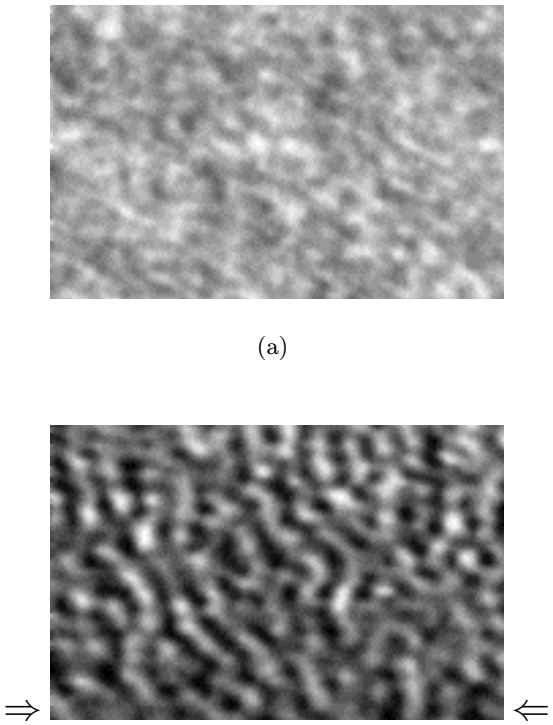

(a)

(b)

Fig. 1. Two BAM images of the monolayer (400 μm$\times$250 μm): a) $\pi \approx 0$ mNm^{-1}; in the unbuckled state, the intensity variations correspond to domains of different tilt orientation. b) $\pi > \pi_c$; the buckled layer shows bright and dark stripes, roughly oriented perpendicular to the compression direction, indicated by arrows.

The intensity level, several orders of magnitude higher than in Figure 1a, cannot be explained only by an in-plane texture: as for direct microscopy, this image is the result of a shadowgraphic process on the rippled interface. We believe that the domain size and the buckling scale are directly related, and the model developed in the following includes the tilt modulation as another relevant parameter for the occurring of the instability.

Light scattering measurements

Since the characteristic buckling length is a few microns, light scattering is well-suited to study the deformation. Our Langmuir trough and experimental set-up for light scattering have been presented elsewhere [5–8]. A laser beamline of wavevector $k = 2\ \pi/\lambda$ hits the surface under a incident angle $\theta_0 = 55°$ with the vertical direction. The buckled interface acts as a grating, and the intensity I_r scattered from the monolayer is detected with a photomultiplier, in the direction $\theta = \theta_0$, at an azimuthal angle ϕ off the specular reflection. The incidence plane is parallel to the compression barriers, and normal to the light polarization. We successively used an argon laser line ($\lambda = 488$ nm, $P_{max} = 35$ mW) and a solid state diode laser ($\lambda = 690$ nm, $P_{max} = 10$ mW). For an interface deformation $\xi(x,y) = \frac{S}{4\pi^2}\int \xi_q \exp(i\mathbf{q}\cdot\mathbf{r})\mathrm{d}^2q$, the scattered intensity per unit solid angle is [9,10]:

$$I(q) = \left(\frac{\mathrm{d}I_r}{\mathrm{d}\Omega}\right) = I_{r0}\frac{k^4}{\pi^2}S\langle|\xi_q|^2\rangle \cos^3\ \theta_0. \qquad (1)$$

This relation is true in the direction of observation ($\theta = \theta_0$, ϕ) and for small q wavevectors related to ϕ by the usual Bragg relation: $q = 2k\sin\theta_0\sin(\phi/2)$. Here I_{r0} is the total reflected intensity in the specular direction. From (1), we expect $|\xi_q|$ to scale like $\sqrt{I(q)}$. Because of the direct reflected light at small angles, we cannot explore the angular domain $|\phi| < \phi_- \approx 1.5°$, corresponding to wavevectors $|q| \leq q_- = 3000$ cm^{-1} at $\lambda = 488$ nm and $|q| \leq q_- = 2000$ cm^{-1} at 690 nm.

Figure 2 shows a given set of experimental spectra recorded from a DSPC film spread on pure formamide, at four successive pressures π. We have normalized $I(q)$ by the value $I(q=0) = I_{r0}$ measured at $\pi = 0$, and plotted $I(q)/I(q=0)$ *versus* the transferred wavevector q. Apart from a central peak corresponding to direct specular reflection, one observes scattered light in the intensity range $I(q)/I(q=0) \approx 10^{-8}$ to 10^{-7}. The lowest curve corresponds to pure formamide without film. With DSPC, there is some scattered light even below the buckling threshold: this may be due to the film texture. As soon as the pressure gets higher than $\pi_c \approx 7 \pm 1$ mN m^{-1}, a complex structure appears: several sharp peaks superimpose to a continuous background. All the peaks appear at the same pressure π_c, they grow with increasing pressure, without any detectable change in position.

In order to make these spectra more readable and to emphasize symmetrical peaks, we first subtract from all spectra an averaged reference spectrum recorded with the film in the unbuckled state at $\pi \approx 0$ mN m^{-1}. Indeed, the spectra recorded at $\pi \approx 0$ are quite reproducible from one run to another. Then we calculate the averaged intensity over two opposite q-values $I_m(q) = \frac{1}{2}[I_s(q) + I_s(-q)]$, with $I_s(q) = \frac{I(q)_{\pi\neq 0} - I(q)_{\pi=0}}{I(q=0)_{\pi=0}}$.

In Figure 3, we have plotted $I_m(q)$ *versus* q from the data of Figure 2. At $\pi = 5$ mN m^{-1}, *i.e.* below the threshold, the mean $I_m(q)$ is zero, as expected. The three other spectra ($\pi = 18$ mN m^{-1}, 30 mN m^{-1}, and 35 mNm^{-1}) still show a complex structure with a set of diffraction peaks.

Repeating this operation for several runs, we have listed the observed peak positions in Table 1. Notice that two runs out of four correspond to $\lambda = 488$ nm, the two others to $\lambda = 690$ nm. Our main conclusions are the following:

i) A family of peaks having approximate harmonic relations and high intensity (in bold characters in Tab. 1) are seen in all the runs. Their average positions are $q = 3500$ cm^{-1}, $2q = 7600$ cm^{-1}, $3q = 12\,000$ cm^{-1} and $4q = 16\,000$ cm^{-1}. The fundamental wavelength is $\lambda = 2\pi/\langle q\rangle = 16.5 \pm 1.5$ μm. Within our accuracy, this wavelength is present in all the experimental runs.

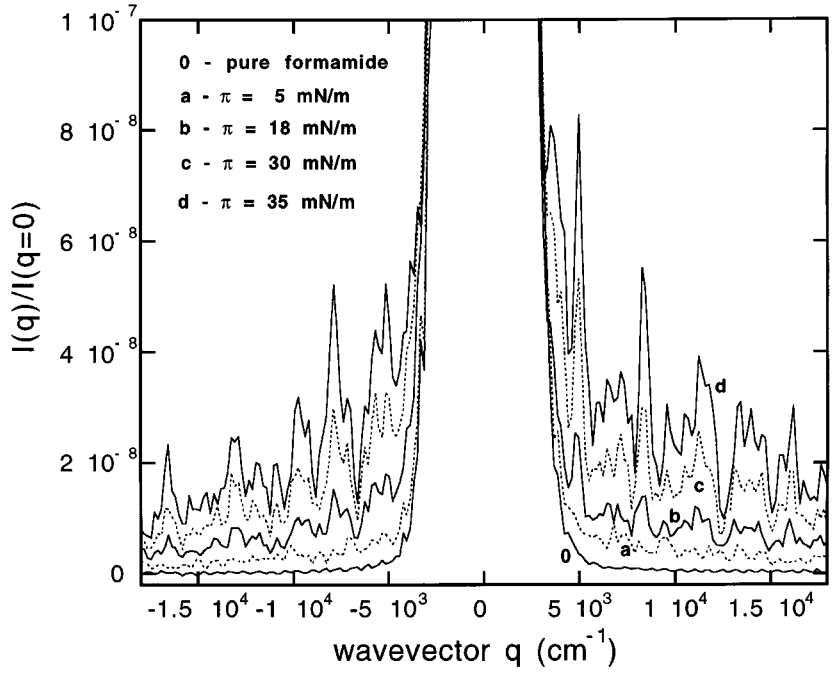

Fig. 2. Scattered intensity $I(q)/I(q = 0)$ plotted *versus* transferred wavevector q, for pure formamide (0), and with a DSPC film at four successive surface pressures (a, b, c, d) ($T = 14$ °C). Several diffraction peaks simultaneously appear at $\pi_c \approx 7$ mN m^{-1}.

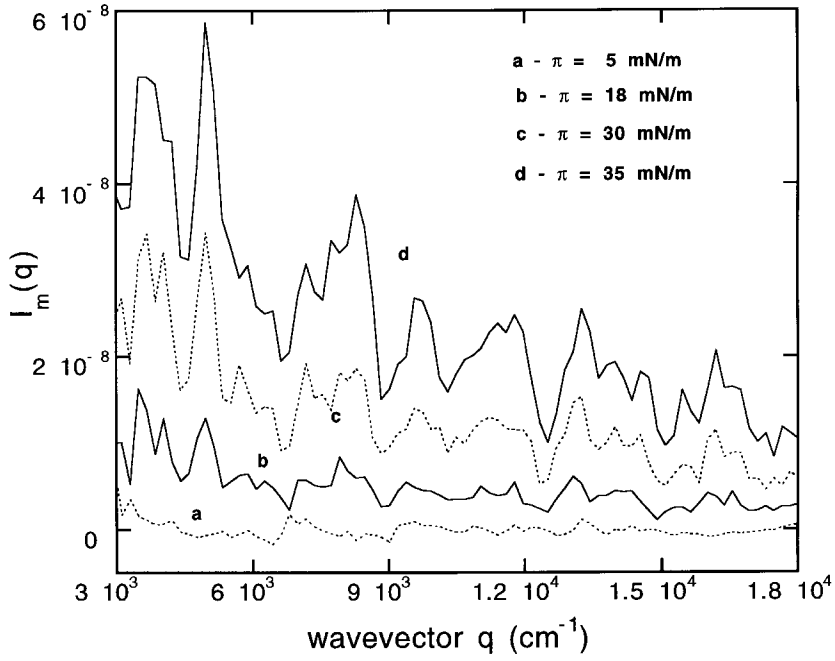

Fig. 3. Averaged scattered intensity $I_m(q)$ (see text) *versus* transferred wavevector q. The intensity increases with increasing pressure, but no global change of the diffraction spectra is observed.

Table 1. Peak positions listed from four set of spectra (Sp1, Sp2, Sp3, Sp4). Each set corresponds to a different DSPC film, and the peak positions are independent of the surface pressure. In bold are the positions of the family of peaks having harmonic relations and seen in all runs.

Sp1		**3600**	4960			**7500**		9750		**11650**	13250	**16200**
Sp2		**3600**	4800		6350	**7700**		9780		**12000**	14500	**16000**
Sp3	2350	**3400**	4500		6050	**7550**	8700		10500	**11900**		**16100**
Sp4	2350	**3350**	4850	5400		**7700**	9000		10200	**12500**	15000	**16200**

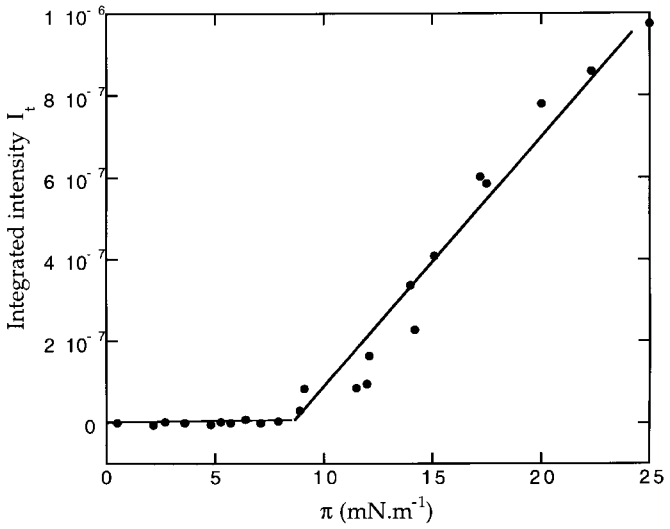

Fig. 4. Plot of the integrated scattered intensity I_t (arbitrary units) *versus* surface pressure π. I_t linearly increases above the pressure threshold $\pi_c = 7$ mN m^{-1}, meaning that the buckling instability is second order.

ii) The other peaks have usually a lower intensity. Their positions do not change in a compression-expansion cycle, but do not appear clearly correlated between them. We observe sometimes harmonic relationships, but this is not reproducible through all the runs.
iii) We always observe that $I(q)$ and thus $I_m(q)$ reversibly follows the pressure variations without any change of the peak positions nor of the global spectrum shape.

We have precisely determined the pressure threshold π_c of the buckling instability in the following way: in Figure 4 we have plotted for a particular run the integrated intensity $I_t = \int_{q_-}^{q_+} I_m(q)dq$ *versus* π. Here $q_+ = 1.8 \times 10^4$ cm^{-1} is the maximum transferred wavevector, approximately corresponding to $\phi = 15°$. For $\pi < \pi_c = 8$ mN m^{-1}, no signal is detected. Above the instability threshold π_c, I_t linearly increases with $\pi - \pi_c$. Averaging over several runs, we found $\pi_c = 7 \pm 1$ mN m^{-1}. Within our accuracy, I_t has no discontinuity at the threshold. Thus we believe that the buckling instability is second order. The fact that the spectra are reversible through compression and expansion enforces this conclusion. At any wavevector q_0 corresponding to a diffraction peak, $I_m(q_0)$ has the same pressure dependence as I_t.

We must here comment the surface pressure threshold and its measurement. It is known that the Wilhelmy plate method does not give correct values in solid phases, all the more as the pressure is likely no longer isotropic. In this way, it is more correct to introduce anisotropic surface stresses.

We have built a capillary wave probe, which is a standard technique to measure surface stresses in different directions [11], in order to investigate the mechanical properties of the DSPC film on formamide. By this technique, we got information on both surface stresses and compression modulus ε. Among other results, we found by this method that the surface stresses are anisotropic above the threshold: the stress is larger in the direction of compression than in the perpendicular one [12].

However, since the monolayer remains isotropic below the threshold, this does not change the value of π_c. In this paper, all surface pressure values measured above π_c are in fact surface stresses measured along the compression direction. This has no incidence on the results concerning the buckling wavelength and amplitude, nor on the theory presented below. A full discussion on surface stress and compression modulus anisotropies will take place in [12].

The vertical deformation amplitude can be estimated from:

$$k^2 \langle |\xi|^2 \rangle \cos^2 \theta_0 = \frac{\pi}{2} \int_0^{\phi_{max}} \frac{\Delta I}{\Delta \Omega I_{r0}} \sin \phi \, d\phi. \quad (2)$$

For our experimental value of the detection solid angle $\Delta\Omega \approx 10^{-5}$ steradian, and taking for simplicity $\Delta I / I_{r0} =$ const. $= 4 \times 10^{-8}$ on the range of $0 < \phi < 10°$ (at $\pi = 30$ mN m^{-1}), we find as an order of magnitude $\Delta\xi = \sqrt{\langle |\xi|^2 \rangle} = 2$ nm. Notice that $\Delta\xi$ varies as $\sqrt{\pi - \pi_c}$ close to the threshold.

As a final remark about the light scattering data, we observed after each compression step a transient relaxation of $I(q)$ towards its equilibrium value. The relaxation time (about one hour) somehow depends on the way the monolayer has been prepared, and is probably related to stress relaxation through defects in the monolayer. Actually, this has no influence on the threshold value nor on the instability wavelength [8].

A model for the buckling instability

Several theoretical approaches have been proposed to explain the buckling instability, either in Langmuir monolayers [5,13,14], or in bilayers [15]. In the case of Langmuir films, the main stabilizing effect at the micrometric scale is the surface tension. Milner *et al.* [13], considering only the balance between surface tension γ and curvature energy κ, predict that the instability occurs at a slightly negative threshold γ_c. Hu and Granek [14] take also into account a possible spontaneous curvature of the film and find that γ_c is positive, but very small compared to our case: remember that the buckling threshold for DSPC on formamide was found equal to $\gamma_c = \gamma_0 - \pi_c = 51$ mN m^{-1}, of the same order of magnitude as γ_0. The main effect of electrostatic dipolar interactions is to renormalize the surface tension, but it does not significantly change the threshold [5]. A more realistic approach takes into account the coupling between the film curvature and the chain tilt angle. Such a coupling may explain the observation of rippled phases in bilayers [15]. Hu and Granek [14] extended this model to monolayers, and found a positive surface tension threshold. However, reasonable values for the elastic coefficients in the tilt texture again lead to a lower surface tension threshold, and a smaller instability wavelength, as compared to our data.

The new model presented in this section develops the following idea: we consider a monolayer presenting a tilt angle θ_0 and a thickness e at equilibrium. We represent

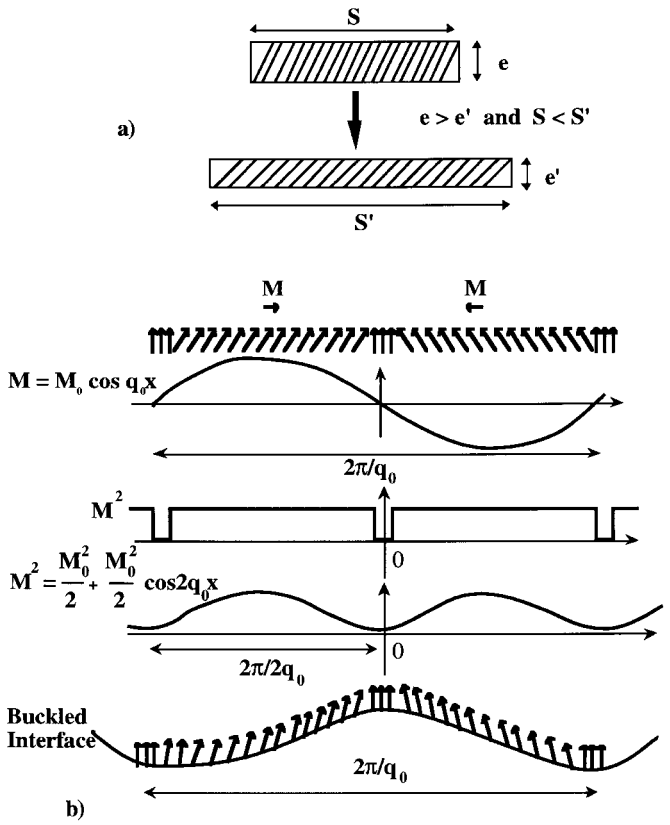

Fig. 5. Model for the instability mechanism. (a) Coupling between the molecular tilt and the film stretching. (b) Variations of the molecular tilt order parameter $M = \sin\theta$ from one domain to the next one, and their schematic representation used in the model.

the tilt projection in the monolayer plane by a vector $\mathbf{M}$ such that $M = \sin\theta$. Any variation ΔM of M around its equilibrium value $M_0 = \sin\theta_0$ induces a layer thickness variation Δe (Fig. 5). It is thus coupled to the total film area S through the 3D elastic coefficients of the monolayer. This model includes what we believe to be important parameters for the instability, *i.e.* the tilt distribution and the high stiffness of DSPC films spread on formamide. The predictions are consistent with our data.

To be quantitative, we consider the 3D elastic energy in the monolayer [16]:

$$E = E_{||} + \frac{K}{2}u_{zz}^2 + \lambda(u_{xx} + u_{yy})u_{zz}. \qquad (3)$$

Here u_{ii} are the diagonal components of the 3D strain tensor, K and λ are Lamé coefficients, $u_{xx} + u_{yy} = \Delta S/S$ represents the surface relative variation, and $u_{zz} = \Delta e/e$ may be related to the variation ΔM of the average tilt angle through:

$$u_{zz} = -\frac{\Delta(M^2)}{2(1 - M_0^2)}\,. \qquad (4)$$

We have not explicited the in-plane elastic energy $E_{||}$, the details of which are not relevant in our case.

Thus $\lambda(u_{xx}+u_{yy})u_{zz}$ appears as the coupling term between layer dilatation and tilt angle variations. The coupling constant λ must be positive, so that stretching the surface induces a film thinning $\Delta e/e < 0$ in order to minimize E (Fig. 5). Now, if we consider thickness variations along the film, the energy will be lowered by making correlated modulations of the in-plane strain and of the tilt angle. Then, the buckling instability will naturally be registered with the strain (and stress) modulation.

A similar argument was previously presented in reference [6]: the authors observed buckling in a polycrystalline polymerized film, and noticed that the buckling scale corresponds to the typical size of the domains. They considered that the surface tension may not be uniform over the film, and suggested that the instability develops because the surface tension vanishes at some places, for instance at the boundaries between domains. This is somehow analogous to the model presented here, which considers a stress modulation and its coupling to the instability.

Now we introduce a deformation $\xi = \sum_q \xi_q \exp(i\mathbf{q}\cdot\mathbf{r})$ of the interface. It corresponds to a surface relative variation $\Delta S/S = (\nabla\xi)^2/2$. Adding to the elastic energy (3) the usual surface tension and bending energy terms, the free energy difference ΔF between a buckled and a flat interface may be written, to second order in ξ:

$$\Delta F = \frac{1}{2}\gamma(\nabla\xi)^2 + \frac{1}{2}\kappa(\Delta\xi)^2 - \frac{1}{4}\lambda(\nabla\xi)^2\frac{\Delta(M^2)}{1 - M_0^2}\,. \qquad (5)$$

Here κ is the bending elastic constant. We have not explicited $E_{||}$, which contains u_{xx}^2 and u_{yy}^2 terms of order ξ^4.

From BAM pictures, we know that the tilt angle is not uniform in the film: it is distributed in domains of estimated size $d = 7 \pm 1$ μm. Thus, even at low pressure, *i.e.* below the buckling threshold, there is a tilt angle distribution which corresponds to a permanent ΔM. From X-ray diffraction data [3], we know that the tilt is locked to the lattice orientation, which is probably random from one crystallite to the next one. In a first step, a very simple approximation consists in considering that the direction of M alternates from one domain to the next one (Fig. 5), and modelling it by its first harmonic along Ox: $M(x) = M_0\cos(q_0 x)$, with $2\pi/q_0 = 2d$. This model can also apply to more regular textures encountered in other systems, like parallel stripes separated by thin boundaries, or mosaic structures [17,18].

Within this crude hypothesis, $M^2(x) = \frac{M_0^2}{2} + \frac{M_0^2}{2}\cos(2q_0 x)$. We first consider a single mode deformation $\xi(x) = \xi_q\cos(qx)$. Therefore, to first order in M_0^2, ΔF becomes:

$$\Delta F = \left[\frac{1}{2}\gamma q^2\cos^2(qx) + \frac{1}{2}\kappa q^4\cos^2(qx) - \frac{1}{4}\lambda q^2\frac{M_0^2}{2 - M_0^2}\left(\frac{1 + \cos(2qx)}{2}\right)\cos(2q_0 x)\right]\xi_q^2. \qquad (6)$$

When q exactly matches the tilt modulation wavevector q_0, $\langle \Delta F \rangle$ presents a minimum $\langle \Delta F \rangle_{\min}$:

$$\langle \Delta F \rangle_{\min} = \left[\left(\gamma - \frac{\lambda}{4} \frac{M_0^2}{(2 - M_0^2)} \right) q_0^2 + \kappa q_0^4 \right] \frac{\xi_{q_0}^2}{4} \cdot \quad (7)$$

A stable deformation ($\xi_{q_0} \neq 0$) develops if γ is below the surface tension threshold γ_c:

$$\gamma_c = \frac{\lambda}{4} \frac{M_0^2}{2 - M_0^2} = \frac{\lambda}{4} \frac{\sin^2 \theta_0}{2 - \sin^2 \theta_0} \cdot \quad (8)$$

In this formula, we have omitted the bending elastic modulus correction $-\kappa q_0^2$, which is negligible at the q_0 scale. We conclude that the elongation-tilt coupling is a destabilizing effect leading to the monolayer buckling at a positive surface tension, at the same wavelength $\Lambda = 2\pi/q_0 = 2d$ as the permanent tilt modulation due to the film texture (d is the domain size). The higher the tilt angle θ_0 and the coupling coefficient λ, the lower the surface pressure buckling threshold $\pi_c = \gamma_0 - \gamma_c$.

According to this model, and from previous determination of $\theta_0 = 35°$ (X-ray diffraction) and $\gamma_c = 51$ mN m^{-1} (light scattering), we estimate the coupling coefficient $\lambda = 1000$ mN m^{-1} at the threshold. This is a reasonable order of magnitude, comparable to the compression modulus of the monolayer $\varepsilon = 3500$ mN m^{-1}, determined by X-ray diffraction [3]. We also expect the buckling wavelength to be identical to the tilt modulation wavelength $\Lambda = 2d = 14 \pm 2$ μm, determined from BAM images. Actually, this is good agreement with light scattering spectra, for which the lower detected harmonic wavelength is $\Lambda = 16.5 \pm 1.5$ μm.

The model is also consistent with the fact that no buckling is observed for DSPC on water. Indeed, in this case the compression modulus of the film is smaller than on formamide ($\varepsilon = 350$ mN/m *versus* 3500 mN/m), and the tilt angle is also smaller. If the coupling parameter λ scales like ε, we expect a much higher pressure threshold for buckling on water, probably above the collapse pressure of the film.

Of course, the model is based on several oversimplified hypothesis and is unable to account for the complexity of the actual light scattering spectra. However, some simple remarks may complete our approach. First, the in-plane tilt distribution cannot be modelled by a simple sinusoïdal function. Therefore, higher harmonics must also appear in the scattered intensity. In principle, it might be possible to retrieve the observed spectra from a direct spectral analysis of the BAM images. Unfortunately, the relevant wavelength is comparable to the BAM resolution, and smaller scale details are not resolved.

A reasonable simulation should consider a regular lattice of domains with a random distribution of tilt orientation. A spectrum computed from such a model is the convolution of the lattice periodic spectrum with the random spectrum of tilt distribution. Preliminary computed spectra resemble the experimentally observed quite closely. Current work is expected to make the comparison quantitative.

Conclusion

In this paper, we have presented a detailed analysis of the buckling instability in a DSPC monolayer at the air-formamide interface, using BAM observations and light scattering measurements. Our interpretation, consistent with the data, relies on the existence of a permanent film texture and a coupling between the tilt angle and the monolayer stretching. We understand the low surface tension threshold and the rather large instability wavelength. Our model could also be quite helpful to describe the rippled phases observed in free bilayers.

We acknowledge Michel Assenheimer for numerous discussions and software assistance, and Sylvie Hénon for her help in BAM experiments.

References

1. S.P. Weinbach, K. Kjaer, J. Als-Nielsen, M. Lahav, L. Leiserowitz, J. Phys. Chem. **97**, 5200 (1993).
2. F. Graner, S. Perez-Oyarzun, A. Saint-Jalmes, C. Flament, F. Gallet, J. Phys. II France **5**, 313-322 (1995).
3. A. Saint-Jalmes, F. Graner, F. Gallet, P. Nassoy, M. Goldmann, Chem. Phys. Lett. **240**, 234 (1995).
4. E. Scalas, H. Möhwald, private communication and unpublished results.
5. A. Saint-Jalmes, F. Graner, F. Gallet, B. Houchmandzadeh, Europhys. Lett. **28**, 565 (1994).
6. L. Bourdieu, J. Daillant, D. Chatenay, A. Braslau, D. Colson, Phys. Rev. Lett. **72**, 1502 (1994).
7. P. Fontaine, J.Daillant, P. Guénoun, M. Alba, A. Braslau, J. W. Mays, J.M. Petit, F. Rieutord, J. Phys. II France **7**, 401-407 (1997).
8. A. Saint-Jalmes, M. Assenheimer, F. Gallet, in *Short and Long Chains at Interfaces* (Éditions Frontières, Gif-sur-Yvette, 1995) p.229.
9. D. Langevin, in *Light scattering by liquid surface and complementary techniques*, edited by D. Langevin, Surfactant science series vol. 41 (M. Dekker, 1992) p. 20 and references therein.
10. P. Croce, J. Optics Paris **8**, 127-139 (1977).
11. K. Miyano, Langmuir **6**, 125 (1990).
12. A. Saint-Jalmes, M. Assenheimer, F. Gallet, submitted to J. Chem. Phys.
13. S.T. Milner, J.-F. Joanny, P. Pincus, Europhys. Lett. **9**, 495 (1989).
14. J.-G. Hu, R. Granek, J. Phys. II France **6**, 999-1022 (1996).
15. C.M. Chen, T.C Lubensky, F.C Mac Kintosh, Phys. Rev. E **51**, 504 (1995).
16. L. Landau and E. Lifchitz, *Theory of Elasticity* (Pergamon Press, Oxford, 1984).
17. S. Hénon, J. Meunier, J. Chem. Phys. **98**, 9148 (1993).
18. D.K. Schwartz, J. Ruiz-Garcia, X. Qiu, J. Selinger, C.M. Knobler, Physica **A204**, 606 (1994).